

Multiwavelength polarization-insensitive lenses based on dielectric metasurfaces with meta-molecules

EHSAN ARBABI, AMIR ARBABI, SEYEDEH MAHSA KAMALI, YU HORIE, AND ANDREI FARAON*

T. J. Watson Laboratory of Applied Physics, California Institute of Technology, 1200 E. California Blvd., Pasadena, California 91125, USA

*Corresponding author: faraon@caltech.edu

Received 25 March 2016; revised 18 May 2016; accepted 24 May 2016 (Doc. ID 261932); published 10 June 2016

Metasurfaces are nanostructured devices composed of arrays of subwavelength scatterers (or meta-atoms) that manipulate the wavefront, polarization, or intensity of light. Like most other diffractive optical devices, metasurfaces are designed to operate optimally at one wavelength. Here, we present a method for designing multiwavelength metasurfaces using unit cells with multiple meta-atoms, or meta-molecules. A transmissive lens that has the same focal distance at 1550 and 915 nm is demonstrated. The lens has a NA of 0.46 and measured focusing efficiencies of 65% and 22% at 1550 and 915 nm, respectively. With proper scaling, these devices can be used in applications where operation at distinct known wavelengths is required, like various fluorescence microscopy techniques. © 2016 Optical Society of America

OCIS codes: (050.6624) Subwavelength structures; (050.1965) Diffractive lenses; (220.1000) Aberration compensation.

<http://dx.doi.org/10.1364/OPTICA.3.000628>

1. INTRODUCTION

Over the last few years, advances in nanofabrication technology have spurred a new wave of interest in diffractive optical elements based on optical metasurfaces [1–5]. From the multiple designs proposed so far, dielectric transmitarrays [6–15] are some of the most versatile metasurfaces because they provide high transmission and subwavelength spatial control of both polarization and phase. Several diffractive optical elements, including high-NA lenses and simultaneous phase and polarization controllers have recently been demonstrated with high efficiencies [10,11]. These devices are based on subwavelength arrays of high-refractive-index dielectric nanoresonators (scatterers) with different geometries, fabricated on a planar substrate. Scatterers with various geometries impart different phases to the transmitted light, shaping its wavefront to the desired form.

One main drawback of almost all of metasurface devices, particularly the ones with spatially varying phase profiles like lenses and gratings, is their chromatic aberration: their performance changes as the wavelength is varied [16–18]. Refractive optical elements also suffer from chromatic aberration; however, their chromatic aberration, which stems from material dispersion, is substantially less than that of the diffractive elements [17,18]. An ideal refractive lens made of a dispersionless material will show no chromatic aberration. On the other hand, the chromatic aberration of diffractive elements mainly comes from the geometrical arrangement of the device. Early efforts focused on making achromatic diffractive lenses by cascading them in the form of doublets and triplets [19–22], but it was later shown that it is

fundamentally impossible to make a converging achromatic lens that has a paraxial solution (i.e., is suitable for imaging) by using only diffractive elements [23]. Although diffractive–refractive combinations have been implemented successfully to reduce chromatic aberration, they are most useful in deep UV and x-ray wavelengths, where materials are significantly more dispersive [24,25].

Truly achromatic diffractive devices have not yet been demonstrated, and recent efforts have focused on demonstration of multiwavelength devices that work at a few distinct wavelengths. For proper operation, a multiwavelength metasurface should provide independent phase control at the desired wavelengths. Multiple resonances of meta-atoms formed from two rectangular dielectric resonators were used in an effort to provide this phase coverage at three wavelengths in [26,27]. However, the demonstrated cylindrical lens, which has a few Fresnel zones and a NA of 0.04, still exhibits multiple focal points. Multiwavelength lenses based on plasmonic metasurfaces were demonstrated in [28,29]. These devices, in addition to the low efficiency of plasmonic metasurfaces [30], have multiple focuses and are polarization dependent. An achromatic metasurface design was proposed in [31] based on the idea of dispersionless meta-atoms (i.e., meta-atoms that impart constant delays). However, this idea only works for metasurface lenses with one Fresnel zone, limiting the size and NA of the lenses. For a typical lens with tens of Fresnel zones, dispersionless meta-atoms will not reduce the chromatic dispersion, as we will discuss shortly. In the following, we briefly discuss the reason for chromatic dispersion of metasurface lenses,

and then propose a method for correcting the lens behavior at distinct wavelengths through complete and independent phase coverage at the design wavelengths. We then experimentally demonstrate a metasurface capable of achieving this completely independent phase control at two wavelengths for the first time to our knowledge, and show polarization-independent single-focus lenses corrected at the two wavelengths. With more complex designs, the method presented in this manuscript can be generalized to multiple wavelengths.

2. THEORY

In diffractive lenses, chromatic dispersion mainly manifests itself through a significant change in focal length as a function of wavelength [24]. This change is schematically shown in Fig. 1(a), along with a schematic metasurface lens assumed to be corrected to have the same focal distance at a few wavelengths. To better understand the underlying reasons for this chromatic dispersion, we consider a hypothetical aspherical metasurface lens. The lens is composed of different meta-atoms that locally modify the phase of the transmitted light to generate the desired wavefront. We assume that the meta-atoms are dispersionless in the sense

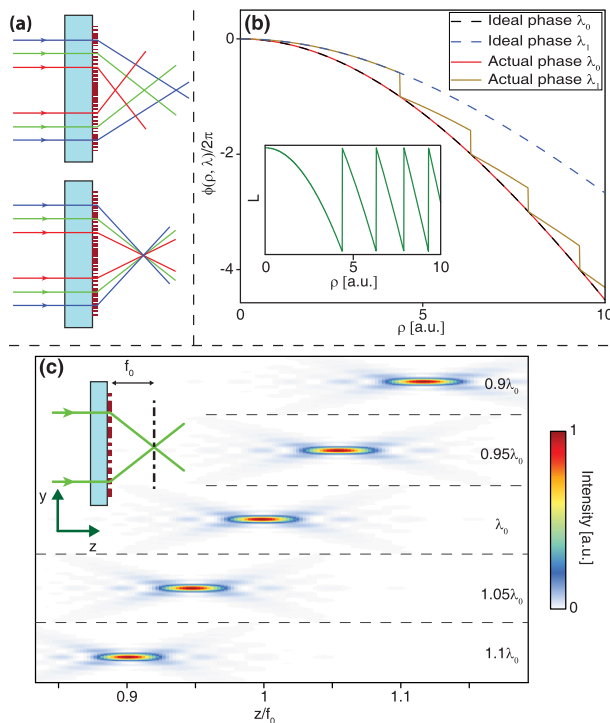


Fig. 1. Chromatic dispersion of metasurface lenses. (a) Schematic illustration of a typical metasurface lens focusing light of different wavelengths to different focal distances (top) and schematic of a metasurface lens corrected to focus light at specific different wavelengths to the same focal distance (bottom), (b) the phase profile of a hypothetical aspherical metasurface lens at the design wavelength λ_0 and a different wavelength λ_1 as a function of the distance to the center of the lens (ρ). Inset: Plot of the parameter of the meta-atoms controlling phase (named L). The Fresnel zone boundaries happen at the integer multiples of 2π in the λ_0 phase curve. These zone boundaries coincide with the jumps in the actual phase at λ_1 and L . (c) Intensity of light at different wavelengths in the axial plane after passing through the lens, showing considerable chromatic dispersion rising from phase jumps at the boundaries between different Fresnel zones.

that their associated phase changes with wavelength as $\phi(\lambda) = 2\pi L/\lambda$, like a piece of dielectric with a constant refractive index. Here λ is the wavelength and L is an effective parameter associated with the meta-atoms that controls the phase (L can be an actual physical parameter or a function of the physical parameters of the meta-atoms). We assume that the full 2π phase needed for the lens is covered using different meta-atoms with different values of L . The lens is designed to focus light at λ_0 [Fig. 1(b)] to a focal distance f_0 , and its phase profile in all Fresnel zones matches the ideal phase profile at this wavelength. Because of the specific wavelength dependence of the dispersionless meta-atoms (i.e., proportionality to $1/\lambda$), at a different wavelength (λ_1) the phase profile of the lens in the first Fresnel zone follows the desired ideal profile needed to maintain the same focal distance [Fig. 1(b)]. However, outside the first Fresnel zone, the actual phase profile of the lens deviates substantially from the desired phase profile. Due to the jumps at the boundaries between the Fresnel zones, the actual phase of the lens at λ_1 is closer to the ideal phase profile at λ_0 than to the desired phase profile at λ_1 . In the inset of Fig. 1(b), the effective meta-atom parameter L is plotted as a function of distance to the center of the lens ρ . The jumps in L coincide with the jumps in the phase profile at λ_1 . In Fig. 1(c), the simulated intensity profile of the same hypothetical lens is plotted at a few wavelengths close to λ_0 . The focal distance changes approximately proportional to $1/\lambda$. This wavelength dependence is also observed in Fresnel zone plates [24], and for lenses with wavelength-independent phase profiles [17,18] (the $1/\lambda$ dependence is exact in the paraxial limit, and approximate in general). This behavior confirms the previous observation that the phase profile of the lens at other wavelengths approximately follows the phase profile at the design wavelength. Therefore, the chromatic dispersion of metasurface lenses mainly stems from wrapping the phase, and also from the dependence of the phase on only one effective parameter (e.g., L) whose value undergoes sudden changes at the zone boundaries. As we show in the following, using two parameters to control metasurface phase at two wavelengths can resolve this issue and enable lenses with the same focal length at two different wavelengths. With more than two control parameters that enable independent phase control at more wavelengths, this idea can be generalized to more than two wavelengths.

3. METASURFACE STRUCTURE

The metasurface platform we use in this work is based on amorphous silicon (α -Si) nanoposts on a fused silica substrate [Fig. 2(a), left]. The nanoposts are placed on the vertices of a hexagonal lattice, and locally sample the phase to generate the desired phase profile [10]. For a fixed height, the transmission phase of a nanopost can be controlled by varying its diameter. The posts' height can be chosen such that at a certain wavelength the whole 2π phase shift is covered, while keeping the transmission amplitude high. Each nanopost has multiple resonances that are excited and contribute to the scattered field with various strengths [32]. Since many resonances play an important role in the response of nanoposts, we find that explaining their response based on these resonances does not provide an intuitive understanding of their operation. Instead, these nanoposts can be better understood as truncated multimode waveguides [32,33]. To design a metasurface that works at two different wavelengths, a unit cell consisting of four different nanoposts [Fig. 2(a), center] was chosen, because

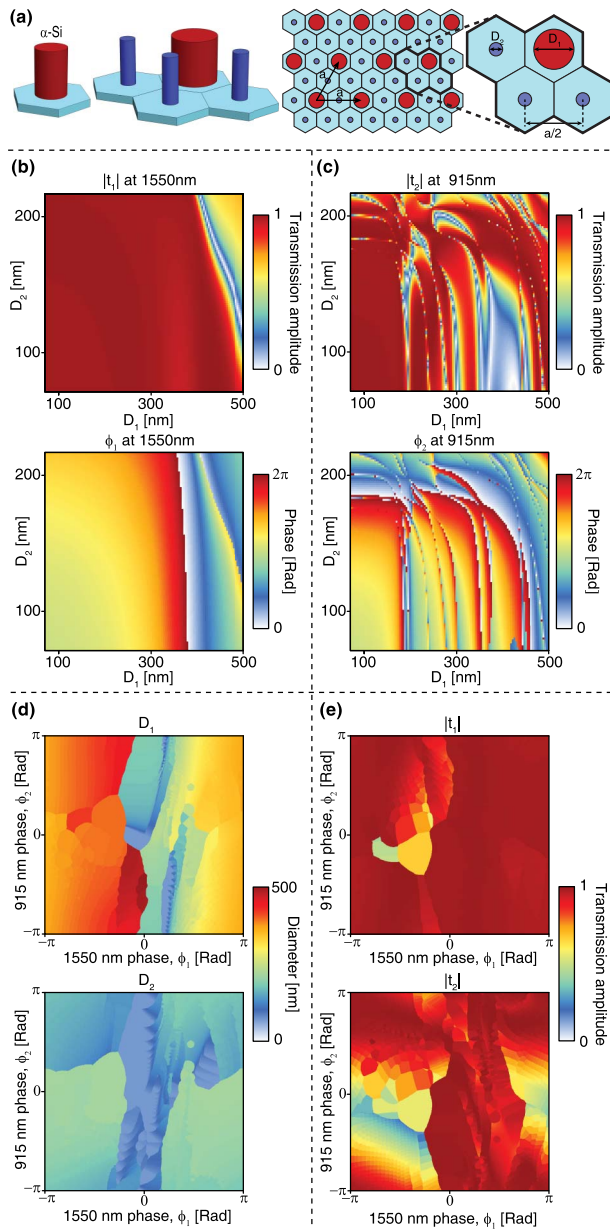


Fig. 2. Meta-molecule design and its transmission characteristics. (a) A single scattering element composed of an α -Si nanopost on a fused silica substrate (left), the unit cell composed of four scattering elements that provide more control parameters for the scattering phase (center), and placement of the meta-molecules on a hexagonal lattice with lattice constant a (right); (b), (c) transmission amplitude (top) and phase (bottom) as a function of the two diameters in the unit cell for 1550 and 915 nm, respectively; (d) selected values of D_1 (top) and D_2 (bottom) as functions of phases at 1550 nm (ϕ_1) and 950 nm (ϕ_2); (e) transmission amplitude at 1550 nm (top) and 915 nm (bottom) for the selected meta-molecules as a function of phase shifts, showing high transmission for almost all phases.

it has more parameters to control the phases at two wavelengths almost independently. Due to the weak coupling between the nanoposts [10], they behave like individual scatterers with large cross-section, as shown in our previous works [10,11,32]. As molecules consisting of multiple atoms form the units for more complex materials, we call these unit cells with multiple meta-atoms

meta-molecules. The meta-molecules can also form a periodic lattice (in this case hexagonal), and effectively sample the desired phase profiles simultaneously at two wavelengths. The lattice is sub-wavelength at both wavelengths of interest; therefore, the nonzero diffraction orders are not excited. In general, the four nanoposts can all have different diameters and distances from each other. However, to make the design process more tractable, we give three of the four nanoposts the same diameter D_2 and the fourth post diameter D_1 , and place them in the centers of the hexagons at a distance $a/2$ [as shown in Fig. 2(a), right]. Therefore, each meta-molecule has two parameters, D_1 and D_2 , to control the phases at two wavelengths. For this demonstration, we choose two wavelengths of 1550 and 915 nm, because of the availability of lasers at these wavelengths. A periodic array of meta-molecules was simulated to find the transmission amplitude and phase (see Section S1 of Supplement 1 for simulation details). The simulated transmission amplitude and phase for 1550 ($|t_1|$ and ϕ_1) and 915 nm ($|t_2|$ and ϕ_2) are plotted as functions of D_1 and D_2 in Figs. 2(b) and 2(c). In these simulations the lattice constant (a) was set to 720 nm, and the posts were 718 nm tall. Since the two wavelengths are not close, the ranges of D_1 and D_2 must be very different in order to properly control the phases at 1550 and 915 nm. For each desired combination of phases ϕ_1 and ϕ_2 in the $(-\pi, \pi)$ range at the two wavelengths, there is a corresponding D_1 and D_2 pair that minimizes the total transmission error, which is defined as $\epsilon = |\exp(i\phi_1) - t_1|^2 + |\exp(i\phi_2) - t_2|^2$. These pairs are plotted in Fig. 2(d) as a function of ϕ_1 and ϕ_2 . Using the complex transmission coefficients (i.e., t_1 and t_2) in error calculations results in automatically avoiding resonance areas where the phase might be close to the desired value but transmission is low. The corresponding transmission amplitudes for the chosen meta-molecules are plotted in Fig. 2(e), and show this automatic avoidance of low-transmission meta-molecules. In the lens design process, the desired transmission phases of the lens are sampled at the lattice points at both wavelengths, resulting in a (ϕ_1, ϕ_2) pair at each lattice site. Using the plots in Fig. 2(d), values of the two post diameters are found for each lattice point. Geometrically, the values of the two diameters are limited by $D_1 + D_2 < a$. In addition, we set a minimum value of 50 nm for the gaps between the posts to facilitate the metasurface fabrication.

4. EXPERIMENTAL RESULTS

A double-wavelength aspherical lens was designed using the proposed platform to operate at both 1550 and 915 nm. The lens has a diameter of 300 μm and focuses the light emitted from single-mode fibers at each wavelength to a focal plane 400 μm away from the lens surface (the corresponding paraxial focal distance is 286 μm , and thus the NA is 0.46). The lens was fabricated using standard nanofabrication techniques: a 718-nm-thick layer of α -Si was deposited on a fused silica substrate, and the lens pattern was generated using electron beam lithography and transferred to the α -Si layer using aluminum oxide as a hard mask (see Section S1 of Supplement 1 for fabrication details). Optical and scanning electron microscope images of the lens and nanoposts are shown in Fig. 3. The smallest diameters of the nanoposts and gap sizes used in the design and fabrication of the metasurfaces were 72 and 50 nm, respectively. For characterization, the fabricated metasurface lens was illuminated by light emitted from the end facet of a single-mode fiber, and

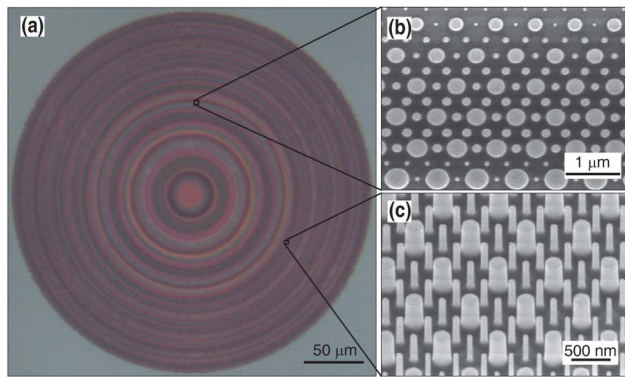


Fig. 3. Fabricated device images. (a) Optical microscope image of the fabricated device; (b), (c) scanning electron micrographs of parts of the fabricated device from top (b) and with a 30 deg tilt (c).

the transmitted light intensity was imaged at different distances from the lens using a custom-built microscope (see Section S1 and Fig. S1 of Supplement 1 for measurement setup and details). Measurement results for both wavelengths are plotted in Figs. 4(a)–4(c). Figures 4(a) and 4(b) show the measured (left) and simulated (right) intensity profiles in the focal plane at 915 and 1550 nm. The measured full width at half-maximum (FWHM) is 1.9 μm at 915 nm and 2.9 μm at 1550 nm. The intensities measured at the two axial plane cross sections are plotted in Fig. 4(c) for the two wavelengths. A nearly diffraction-limited focus is observed in the measurements, and no other secondary focal points with comparable intensity are seen. To confirm the diffraction-limited behavior, a perfect phase mask was simulated using the same illumination as the measurements. The simulated FWHMs were 1.6 and 2.75 μm for 915 and 1550 nm, respectively (see Section S1 of Supplement 1 for simulation details). Focusing efficiencies of 22% and 65% were measured for 915 and 1550 nm, respectively. Focusing efficiency is defined as the ratio of the power passing through a 20- μm -diameter disk around the focus to the total power incident on the lens. As expected from the lattice and lens symmetries, no measurable change in the focus pattern or efficiency of the lens was observed as the incident light polarization was varied. Another lens with a longer focal distance of 1000 μm (thus a lower NA of 0.29) was fabricated and measured with the same platform and method. Measurement results for those devices are presented in Fig. S2 of Supplement 1. Slightly higher focusing efficiencies of 25% and 72% were measured at 915 and 1550 nm, respectively, for those devices. For comparison, a lens designed with the same method and based on the same metasurface platform is simulated using the finite-difference time-domain (FDTD) method with freely available software (MEEP) [34]. To reduce the computational cost, the simulated lens is four times smaller and focuses the light at a 100 μm distance. Because of the equal NAs of the simulated and fabricated devices, the focal intensity distributions and the focal depths are comparable. The simulation results are shown in Figs. 4(a), 4(b), and 4(d). Figures 4(a) and 4(b) show the simulated focal plane intensity of the lens at 915 and 1550 nm, respectively. The simulated FWHM is 1.9 μm at 915 nm and 3 μm at 1550 nm, both of which are in accordance with their corresponding measured values. Also, the simulated intensity distributions in the axial cross

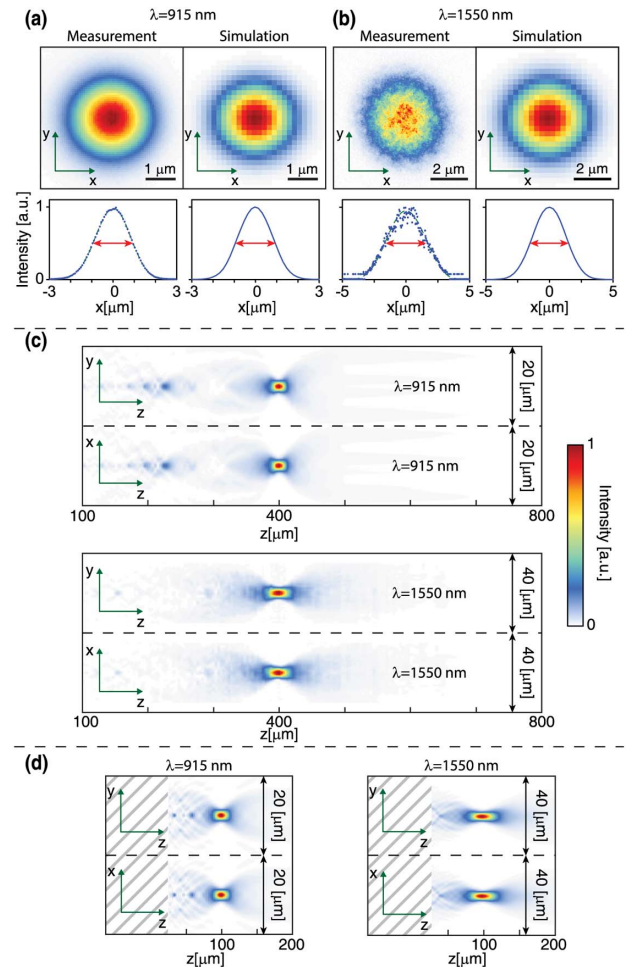


Fig. 4. Measurement and simulation results of the double-wavelength lenses. (a) Measured (left) and simulated (right) focal plane intensities at 915 nm. The simulated lens has the same NA as the measured one but is four times smaller. One-dimensional cross sections of the measured and simulated intensity profiles are shown at the bottom. The red arrows denote the FWHMs, which are both ~ 1.9 μm . (b) Same results as in (a), but for 1550 nm. The high frequency fluctuations seen in the measured intensity are caused by the highly nonuniform sensitivity of the phosphorus-coated CCD camera. The FWHMs are ~ 2.9 and ~ 3 μm for the measurement and simulation, respectively. (c) Intensity measured in the axial planes of the lens for 915 nm (top) and 1550 nm (bottom). The high frequency noise of the camera at 1550 nm is filtered to generate a smooth distribution. (d) Simulated intensity profiles in the axial planes at 915 nm (left) and 1550 nm (right) for the four-times-smaller lens.

section planes, which are shown in Fig. 4(d), demonstrate only one strong focal point. The focusing efficiency was found to be 32% at 915 nm and 73% at 1550 nm. We attribute the differences between the simulated and measured efficiencies to fabrication imperfections and measurement artifacts (see Section S1 of Supplement 1 for measurement details).

5. DISCUSSION

The efficiency at 915 nm is found to be lower than was expected in both measurement and FDTD simulation. While the average power transmission of the selected meta-molecules is about 73%, as calculated from Fig. 2(e), the simulated focusing efficiency is

about 32%. To better understand the reasons for this difference, two blazed gratings with different angles were designed and simulated for both wavelengths using the same meta-molecules (see Section S2 and Fig. S3 of Supplement 1). It is observed that for the gratings (that are aperiodic), a significant portion of the power is diffracted to other angles both in reflection and transmission. In addition, the power lost to diffractions to other angles is higher for the grating with a larger deflection angle. The main reason for the large power loss to other angles is the relatively large lattice constant. The chosen lattice constant of $a = 720$ nm is just slightly smaller than $a_{\max} = \frac{2}{\sqrt{3}n_g}\lambda = 727$ nm, the lattice constant at which the first-order diffracted light starts to propagate in the glass substrate (refractive index: $n_g = 1.452$) for a perfectly periodic structure. Thus, even a small deviation from perfect periodicity can result in light being diffracted to propagating orders. Also, the lower transmission of some meta-molecules reduces the purity of the plane wave wavefronts diffracted to the design angle. Furthermore, the desired phase profile of high-NA lenses cannot be sampled at a high enough resolution using large lattice constants. Therefore, as shown in this work, a lens with a lower NA has a higher efficiency. There are a few methods of increasing the efficiency of the lenses at 915 nm: the lattice constant is bound by the geometrical and fabrication constraint, $D_1 + D_2 + 100$ nm $< a$, and hence the smallest value of $D_1 + D_2$ that gives full phase coverage at the longer wavelength sets the lower bound for the lattice constant. This limit can usually be decreased by using taller posts; however, that would result in a high sensitivity to fabrication errors at the shorter wavelength. Thus, a compromise should be made here, and higher-efficiency designs might be possible through more optimal selections of the posts' height and the lattice constant. The lattice constant can also be smaller if less than the full 2π phase shift is used at 1550 nm (thus a lower efficiency at 1550 nm). In addition, as explained earlier, in minimizing the total transmission error, equal weights are used for 915 and 1550 nm. A higher weight for 915 nm might result in higher efficiency at this wavelength, probably at the expense of the 1550 nm efficiency. For instance, if we optimize the lens only for operation at 915 nm, devices with efficiencies as high as 80% are possible [10,11].

Utilizing more degrees of freedom in the unit cell can increase the number of wavelengths with independent phase control. While each different diameter of the nanoposts in the unit cell can be used to add an additional wavelength with independent control, other geometrical parameters in the unit cell might enable additional control. Increasing the number of wavelengths will probably result in a decreased efficiency at each wavelength, as the transmission phase and amplitude errors at each individual wavelength will probably increase. We reserve a more detailed study of these effects for later work.

The approach presented here (similar to other approaches presented in other works so far) cannot be directly used to correct for chromatic dispersion over a continuous bandwidth; the multiwavelength lenses still have chromatic dispersion, much like normal metasurface lenses in narrow bandwidths around the corrected wavelengths. To achieve zero chromatic dispersion over a narrow bandwidth, the meta-atoms should independently control the phase at two very close wavelengths. High-quality-factor resonances must be present for the meta-atom phase to change rapidly over a narrow bandwidth, and such resonances will result in high

sensitivity to fabrication errors, which would make the metasurface impractical.

6. CONCLUSION

The meta-molecule platform, used here to correct for chromatic aberration at specific wavelengths, can also be used for applications where different functionalities at different wavelengths are desired. For instance, it can be used to implement a lens with two given focal distances at two wavelengths, or a lens converging at one wavelength and diverging at the other. In addition, given the generality of the meta-molecule concept, it can be applied to other areas of interest in metasurfaces (such as nonlinear [35–37] and microwave [38,39] metasurfaces). Multiwavelength operation is necessary in various microscopy applications where fluorescence is excited at one wavelength and collected at another. In this work we have used only two of the degrees of freedom of the meta-molecules, but increased functionality at more than two wavelengths can be achieved by making use of all the degrees of freedom. Operation at more than two wavelengths enables application in color display technologies or more complex fluorescence imaging techniques.

Funding. National Science Foundation (NSF) (1512266); Samsung; Defense Advanced Research Projects Agency (DARPA); U.S. Department of Energy (DOE) (DE-SC0001293).

Acknowledgment. The device nanofabrication was performed at the Kavli Nanoscience Institute at Caltech.

See Supplement 1 for supporting content.

REFERENCES

1. A. V. Kildishev, A. Boltasseva, and V. M. Shalaev, "Planar photonics with metasurfaces," *Science* **339**, 1232009 (2013).
2. N. Yu and F. Capasso, "Flat optics with designer metasurfaces," *Nat. Mater.* **13**, 139–150 (2014).
3. S. Jahani and Z. Jacob, "All-dielectric metamaterials," *Nat. Nanotechnol.* **11**, 23–36 (2016).
4. D. Fattal, J. Li, Z. Peng, M. Fiorentino, and R. G. Beausoleil, "Flat dielectric grating reflectors with focusing abilities," *Nat. Photon.* **4**, 466–470 (2010).
5. D. Lin, P. Fan, E. Hasman, and M. L. Brongersma, "Dielectric gradient metasurface optical elements," *Science* **345**, 298–302 (2014).
6. S. Astilean, P. Lalanne, P. Chavel, E. Cambriil, and H. Launois, "High-efficiency subwavelength diffractive element patterned in a high-refractive-index material for 633 nm," *Opt. Lett.* **23**, 552–554 (1998).
7. P. Lalanne, S. Astilean, P. Chavel, E. Cambriil, and H. Launois, "Design and fabrication of blazed binary diffractive elements with sampling periods smaller than the structural cutoff," *J. Opt. Soc. Am. A* **16**, 1143–1156 (1999).
8. S. Vo, D. Fattal, W. V. Sorin, P. Zhen, T. Tho, M. Fiorentino, and R. G. Beausoleil, "Sub-wavelength grating lenses with a twist," *IEEE Photon. Technol. Lett.* **26**, 1375–1378 (2014).
9. P. R. West, J. L. Stewart, A. V. Kildishev, V. M. Shalaev, V. V. Shkunov, F. Strohkendl, Y. A. Zakharenkov, R. K. Dodds, and R. Byren, "All-dielectric subwavelength metasurface focusing lens," *Opt. Express* **22**, 26212–26221 (2014).
10. A. Arbabi, Y. Horie, A. J. Ball, M. Bagheri, and A. Faraon, "Subwavelength-thick lenses with high numerical apertures and large efficiency based on high-contrast transmitarrays," *Nat. Commun.* **6**, 7069 (2015).
11. A. Arbabi, Y. Horie, M. Bagheri, and A. Faraon, "Dielectric metasurfaces for complete control of phase and polarization with subwavelength

- spatial resolution and high transmission," *Nat. Nanotechnol.* **10**, 937–943 (2015).
12. M. Decker, I. Staude, M. Falkner, J. Dominguez, D. N. Neshev, I. Brener, T. Pertsch, and Y. S. Kivshar, "High-efficiency dielectric Huygens' surfaces," *Adv. Opt. Mater.* **3**, 813–820 (2015).
 13. Y. F. Yu, A. Y. Zhu, R. Paniagua-Domínguez, Y. H. Fu, B. Luk'yanchuk, and A. I. Kuznetsov, "High-transmission dielectric metasurface with 2π phase control at visible wavelengths," *Laser Photon. Rev.* **9**, 412–418 (2015).
 14. S. Campione, L. I. Basilio, L. K. Warne, and M. B. Sinclair, "Tailoring dielectric resonator geometries for directional scattering and Huygens' metasurfaces," *Opt. Express* **23**, 2293–2307 (2015).
 15. M. I. Shalaev, J. Sun, A. Tsukernik, A. Pandey, K. Nikolskiy, and N. M. Litchinitser, "High-efficiency all-dielectric metasurfaces for ultracompact beam manipulation in transmission mode," *Nano Lett.* **15**, 6261–6266 (2015).
 16. M. Young, "Zone plates and their aberrations," *J. Opt. Soc. Am.* **62**, 972–976 (1972).
 17. M. Born and E. Wolf, *Principles of Optics: Electromagnetic Theory of Propagation, Interference and Diffraction of Light* (Cambridge University, 1999).
 18. B. Saleh and M. Teich, *Fundamentals of Photonics* (Wiley, 2013).
 19. J. N. Latta, "Analysis of multiple hologram optical elements with low dispersion and low aberrations," *Appl. Opt.* **11**, 1686–1696 (1972).
 20. S. J. Bennett, "Achromatic combinations of hologram optical elements," *Appl. Opt.* **15**, 542–545 (1976).
 21. W. Sweatt, "Achromatic triplet using holographic optical elements," *Appl. Opt.* **16**, 1390–1391 (1977).
 22. I. Weingärtner and K.-J. Rosenbruch, "Chromatic correction of two- and three-element holographic imaging systems," *Opt. Acta* **29**, 519–529 (1982).
 23. D. A. Buralli and J. R. Rogers, "Some fundamental limitations of achromatic holographic systems," *J. Opt. Soc. Am. A* **6**, 1863–1868 (1989).
 24. G. J. Swanson, "Binary optics technology: the theory and design of multi-level diffractive optical elements," Tech. Rep. 854, DTIC Document (MIT Lincoln Laboratory, 1989).
 25. Y. Wang, W. Yun, and C. Jacobsen, "Achromatic Fresnel optics for wide-band extreme-ultraviolet and x-ray imaging," *Nature* **424**, 50–53 (2003).
 26. F. Aieta, M. A. Kats, P. Genevet, and F. Capasso, "Multiwavelength achromatic metasurfaces by dispersive phase compensation," *Science* **347**, 1342–1345 (2015).
 27. M. Khorasaninejad, F. Aieta, P. Kanhaiya, M. A. Kats, P. Genevet, D. Rousso, and F. Capasso, "Achromatic metasurface lens at telecommunication wavelengths," *Nano Lett.* **15**, 5358–5362 (2015).
 28. O. Eisenbach, O. Avayu, R. Ditzovski, and T. Ellenbogen, "Metasurfaces based dual wavelength diffractive lenses," *Opt. Express* **23**, 3928–3936 (2015).
 29. Z. Zhao, M. Pu, H. Gao, J. Jin, X. Li, X. Ma, Y. Wang, P. Gao, and X. Luo, "Multispectral optical metasurfaces enabled by achromatic phase transition," *Sci. Rep.* **5**, 15781 (2015).
 30. A. Arbabi and A. Faraon, "Fundamental limits of ultrathin metasurfaces," arXiv:1411.2537 (2014).
 31. J. Cheng and H. Mosallaei, "Truly achromatic optical metasurfaces: a filter circuit theory-based design," *J. Opt. Soc. Am. B* **32**, 2115–2121 (2015).
 32. S. M. Kamali, A. Arbabi, E. Arbabi, Y. Horie, and A. Faraon, "Decoupling optical function and geometrical form using conformal flexible dielectric metasurfaces," *Nat. Commun.* **7**, 11618 (2016).
 33. P. Lalanne, "Waveguiding in blazed-binary diffractive elements," *J. Opt. Soc. Am. A* **16**, 2517–2520 (1999).
 34. A. F. Oskooi, D. Roundy, M. Ibanescu, P. Bermel, J. D. Joannopoulos, and S. G. Johnson, "MEEP: a flexible free-software package for electromagnetic simulations by the FDTD method," *Comput. Phys. Commun.* **181**, 687–702 (2010).
 35. M. Tymchenko, J. S. Gomez-Diaz, J. Lee, N. Nookala, M. A. Belkin, and A. Alù, "Gradient nonlinear Pancharatnam-Berry metasurfaces," *Phys. Rev. Lett.* **115**, 207403 (2015).
 36. O. Wolf, S. Campione, A. Benz, A. P. Ravikumar, S. Liu, T. S. Luk, E. A. Kadlec, E. A. Shaner, J. F. Klem, M. B. Sinclair, and I. Brener, "Phased-array sources based on nonlinear metamaterial nanocavities," *Nat. Commun.* **6**, 7667 (2015).
 37. N. Nookala, J. Lee, M. Tymchenko, J. S. Gomez-Diaz, F. Demmerle, G. Boehm, K. Lai, G. Shvets, M.-C. Amann, A. Alu, and M. Belkin, "Ultrathin gradient nonlinear metasurface with a giant nonlinear response," *Optica* **3**, 283–288 (2016).
 38. C. Pfeiffer and A. Grbic, "Metamaterial Huygens' surfaces: tailoring wave fronts with reflectionless sheets," *Phys. Rev. Lett.* **110**, 197401 (2013).
 39. A. Epstein, J. P. S. Wong, and G. V. Eleftheriades, "Cavity-excited Huygens' metasurface antennas for near-unity aperture illumination efficiency from arbitrarily large apertures," *Nat. Commun.* **7**, 10360 (2016).